Chemistry of Metals and Alloys

Chem. Met. Alloys 4 (2011) 234-242
Ivan Franko National University of Lviv
www.chemetal-journal.org

Interaction between the components in the {Zr, Hf}-Ag-Sn ternary systems

N. MELNYCHENKO-KOBLYUK[1], V.V. ROMAKA[2], L. ROMAKA[1]*, Yu. STADNYK[1]

[1] *Department of Inorganic Chemistry, Ivan Franko National University of Lviv, Kyryla i Mefodiya St. 6, 79005 Lviv, Ukraine*
[2] *Department of Materials Engineering and Applied Physics, Lviv Polytechnic National University, Ustyyanovycha St. 5, 79013 Lviv, Ukraine*
* *Corresponding author. E-mail: romakal@franko.lviv.ua*

Received April 4, 2011; accepted December 28, 2011; available on-line August 17, 2012

The phase equilibria in the Zr–Ag–Sn and Hf–Ag–Sn ternary systems at 770 K and 870 K, respectively, were studied by means of X-ray diffraction and metallographic analysis over the whole concentration range. At the temperatures of the investigations the presence of ternary phases was observed neither in the Zr–Ag–Sn, nor in the Hf–Ag–Sn system. Significant solid solutions based on the Zr_5Sn_4 and Hf_5Sn_4 binaries (Ti_5Ga_4 type, space group $P6_3/mcm$) were found in both the investigated systems. The limiting compositions of the solid solutions (Zr_5AgSn_3 and Hf_5AgSn_3) are considered as compounds with Hf_5CuSn_3 structure type. The regions of existence and the cell parameters of the $Zr_5Ag_xSn_{4-x}$ and $Hf_5Ag_xSn_{4-x}$ (x = 0.0-1.0) solid solutions were determined using EMPA and X-ray powder diffraction.

Stannides / Phase diagrams / Solid solution / X-ray diffraction / EPMA

1. Introduction

Our recent systematic studies have covered phase diagrams, crystal chemistry and physical properties of intermediate ternary phases in ternary systems with elements of the 4b-subgroup (Zr, Hf), transition metals and tin [1-7]. For some ternary systems, *i.e.* Zr–Co–Sn [1], Hf–Co–Sn [2], Zr–Ni–Sn [3], Hf–Ni–Sn [4], Zr–Cu–Sn [5], and Hf–Cu–Sn [6], the phase diagrams were studied over the whole concentration range. A maximum of four compounds was found in the {Zr, Hf}–{Co, Ni}–Sn systems, whereas in the {Zr, Hf}–Cu–Sn systems only two ternary phases were observed.

All the studied systems are characterized by the presence of equiatomic compounds. The *Me*NiSn stannides (*Me* = Zr, Hf) crystallize in the cubic MgAgAs type, and are perspective semiconducting materials for thermoelectric applications [8,9]. In the {Zr, Hf}–{Co, Cu}–Sn systems the equiatomic compounds are characterized by different structure types: ZrCoSn and HfCoSn crystallize in the hexagonal ZrNiAl type, while ZrCuSn and HfCuSn crystallize in the TiNiSi and LiGaGe type, respectively.

Sn–Zr and Ag-doped Sn–Zr alloys have been intensively studied by electrochemical measurements, as perspective anode materials [10]. Thus, the investigation of the phase relations in the {Zr, Hf}–Ag–Sn systems is very important for understanding the influence of the method of preparation, heat treatment, and atomic size criteria, on the crystal structures, composition and stability of the formed compounds.

The ternary Zr–Ag–Sn and Hf–Ag–Sn systems have not been investigated up to now. In this paper we present for the first time the results of X-ray diffraction and EPMA analyses of the phase equilibria in the Zr–Ag–Sn and Hf–Ag–Sn ternary systems at 770 K and 870 K, respectively.

2. Experimental

The samples were prepared by arc-melting the constituent elements (the purity of zirconium, hafnium and silver was 99.99 wt.%, the purity of tin was 99.999 wt.%.) under purified, Ti-gettered, argon atmosphere, using a non-consumable tungsten electrode on a water-cooled copper hearth. The overall weight losses were generally less than 1 wt.%. The alloys were annealed at 770 K for samples with zirconium and

Table 1 Crystallographic characteristics of unary and binary phases in the Zr–Ag, Ag–Sn and Zr–Sn systems at 770 K.

Phase	Pearson symbol	Space group	Structure type	Lattice parameters, nm			Reference
				a	*b*	*c*	
(Zr)	*hP*2	*P*6$_3$/*mmc*	Mg	0.3227	–	0.5142	[14]
				0.3218(1)	–	0.5162(2)	this work
Zr_2Ag	*tI*6	*I*4/*mmm*	Zr_2Cu	0.323	–	1.195	[15]
				0.3246(2)	–	1.1923(4)	this work
ZrAg	*tP*4	*P*4/*nmm*	TiCu	0.3471	–	0.6603	[16]
				0.3469(2)	–	0.6589(3)	this work
(Ag)	*cF*4	*Fm*-3*m*	Cu	0.4080	–	–	[14]
$Ag_{1-x}Sn_x$ (x = 0.0-0.1)	*cF*4	*Fm*-3*m*	Cu	0.4065(3)-0.4095(4)	–	–	this work
$Ag_{0.8}Sn_{0.2}$ (12.3-22.2 at.% Sn)	*hP*2	*P*6$_3$/*mmc*	Mg	0.29658	–	0.47824	[17]
				0.2956(1)-0.2983(2)	–	0.4752(2)-0.4750(2)	this work
(Sn)	*tI*4	*I*4$_1$/*amd*	Sn	0.58300	–	0.31802	[18]
				0.5814(2)	–	0.3173(1)	this work
$ZrSn_2$	*oF*24	*Fddd*	$TiSi_2$	0.56434	0.9377	0.99287	[19]
				0.5612(1)	0.9543(1)	0.9881(1)	this work
Zr_5Sn_4	*hP*18	*P*6$_3$/*mcm*	Ti_5Ga_4	0.87656(7)	–	0.5937(1)	[19]
				0.8456(4)	–	0.5784(5)	this work
Zr_5Sn_3	*hP*16	*P*6$_3$/*mcm*	Mn_5Si_3	0.84560(7)	–	0.5779(1)	[19]
				0.8431(3)	–	0.5723(4)	this work
$Zr_{3.2}Sn_{0.8}$	*cP*8	*Pm*-3*n*	Cr_3Si	0.56254	–	–	[19]
				0.5622(3)	–	–	this work

870 K for samples with hafnium for 720 h in evacuated quartz ampoules, and finally quenched in cold water.

Phase analysis was performed using X-ray powder diffraction patterns of the synthesized samples (DRON-2.0M, Fe *Kα* radiation). The observed diffraction intensities were compared with reference powder patterns of the unary and known binary phases. The compositions of the obtained samples were examined by Scanning Electron Microscopy (SEM) using a Carl Zeiss DSM 962 scanning microscope with a Link EDX system operating at 20 kV and 60 μA. Quantitative electron probe microanalysis (EPMA) of the phases was carried out by using an energy-dispersive X-ray analyzer with the pure elements as standards (the acceleration voltage was 20 kV; *K*- and *L*-lines were used).

Calculations of the unit cell parameters and theoretical patterns were performed using the CSD [11] and PowderCell [12] program packages. Rietveld refinements of the crystal structures were performed using the WinPLOTR program package [13].

3. Results and discussion

3.1. Isothermal section of the Zr–Ag–Sn system

The phase equilibria of the Zr–Ag–Sn ternary system at 770 K were investigated based on X-ray diffraction and electron probe microanalysis of 42 binary and ternary alloys.

The binary systems Zr–Ag, Ag–Sn and Zr–Sn, which delimit the ternary Zr–Ag–Sn system, have been investigated earlier and their phase diagrams are already known [14-19]. The presence of almost all of the binary compounds reported at 770 K in the Zr–Ag (Zr_2Ag, ZrAg), Ag–Sn ($Ag_{0.8}Sn_{0.2}$) and Zr–Sn ($ZrSn_2$, Zr_5Sn_4, Zr_5Sn_3, $Zr_{3.2}Sn_{0.8}$) systems, was confirmed. Crystallographic characteristics of the unary and binary phases in the systems Zr–Ag, Ag–Sn and Zr–Sn at 770 K are listed in Table 1. The $Ag_{0.8}Sn_{0.2}$, Zr_2Ag, and ZrAg binary compounds are characterized by small homogeneity regions (Table 1), but the solubility of the third component in these compounds is less than 1-2 at.%.

In the Zr–Ag–Sn system a single-phase sample with composition ~$Zr_{56}Ag_{11}Sn_{33}$ was obtained.

Table 2 EPMA and crystallographic data for selected Zr–Ag–Sn alloys annealed at 770 K.

Nominal composition	Phase	Structure type	Lattice parameters, nm			EPMA, at.%		
			a	*b*	*c*	Zr	Ag	Sn
$Zr_{45}Ag_{25}Sn_{30}$ (a)	Zr_5AgSn_3	Hf_5CuSn_3	0.8445(3)	–	0.5768(3)	56.70	11.55	31.75
	(Ag)	Cu	0.4097(2)	–	–	1.94	94.29	3.77
$Zr_{20}Ag_{60}Sn_{20}$ (b)	$Ag_{0.8}Sn_{0.2}$	Mg	0.2971(2)	–	0.4750(2)	1.44	80.01	18.55
	Zr_5AgSn_3	Hf_5CuSn_3	0.8446(3)	–	0.5768(4)	55.70	11.31	32.99
$Zr_{40}Ag_{40}Sn_{20}$ (c)	ZrAg	TiCu	0.3469(2)	–	0.6589(3)	48.11	51.29	0.6
	Zr_5AgSn_3	Hf_5CuSn_3	0.8445(1)	–	0.5767(2)	55.22	11.42	33.36
	(Ag)	Cu	0.4095(1)	–	–	1.42	96.81	1.77
$Zr_{70}Ag_{15}Sn_{15}$	(Zr)	Mg	0.3218(1)	–	0.5161(3)			
	Zr_5AgSn_3	Hf_5CuSn_3	0.8445(3)	–	0.5768(5)			
	Zr_2Ag	Zr_2Cu	0.3246(2)	–	1.1923(4)			
$Zr_{20}Ag_{40}Sn_{40}$ (d)	$Ag_{0.8}Sn_{0.2}$	Mg	0.2980(2)	–	0.4750(2)	0.93	77.93	21.14
	Zr_5AgSn_3	Hf_5CuSn_3	0.8446(3)	–	0.5769(2)			
	$ZrSn_2$	$TiSi_2$	0.5612(1)	0.9543(1)	0.9881(1)	32.34	0.88	66.78
$Zr_{20}Ag_{20}Sn_{60}$	$Ag_{0.8}Sn_{0.2}$	Mg	0.2983(2)	–	0.4750(2)			
	$ZrSn_2$	$TiSi_2$	0.5610(1)	0.9542(1)	0.9881(1)			
	(Sn)	Sn	0.5814(2)	–	0.3173(1)			

* a, b, c, d correspond to samples in Fig. 1.

The powder pattern reflections of the $Zr_{56}Ag_{11}Sn_{33}$ sample were indexed in space group $P6_3/mcm$ with cell parameters a = 0.8414(1) nm, c = 0.5761(2) nm. The observed intensities were corroborated by calculation assuming this phase to have Hf_5CuSn_3 type (space group $P6_3/mcm$) with two Ag atoms in position 2*b*, six Sn in 6*g*, and ten Zr in 4*d* and 6*g*.

The existence of the binary compounds Zr_5Sn_3 (Mn_5Si_3-type) and Zr_5Sn_4 (Ti_5Ga_4-type) has been reported in [19]. The authors analyzed in detail the Zr_5Sn_3–Zr_5Sn_4 binary region and proposed that these two phases are stoichiometric 5:3 and 5:4 compounds at low temperature, and form a solid solution of the Zr_5Sn_{3+x} type at higher temperatures (T > 1373 K). The Ti_5Ga_4 structure type may be considered as a Mn_5Si_3 type with an additional position 2*b*, allowing the formation of a solid solution where the Sn atoms are added into the Zr_5Sn_3 host according to the formula Zr_5Sn_{3+y} (y = 0.0-1.0). In this case a transformation from the Mn_5Si_3 type (Zr_5Sn_3 compound) to the Ti_5Ga_4 type (Zr_5Sn_4 compound) takes place.

The Hf_5CuSn_3 structure type can be obtained by inclusion of Cu atoms into the octahedral voids of the Mn_5Si_3 structure type (two vacancies in the unit cell) [20,21]. On the other hand, the Hf_5CuSn_3 structure can be considered as a superstructure of the Ti_5Ga_4 type, which is obtained by adding Ga atoms into the same voids of the Mn_5Si_3 structure type [22]. Zr_5AgSn_3 corresponds to the extreme composition, either of a solid solution with substitution of Ag for Sn in the Zr_5Sn_4 binary compound (Ti_5Ga_4-type), or of a solid solution where Ag atoms are added into Zr_5Sn_3 (Mn_5Si_3-type).

We prepared additional alloys in the region Zr_5AgSn_3–Zr_5Sn_3–Zr_5Sn_4 in order to examine the process of solid solution formation between Zr_5AgSn_3, Zr_5Sn_3 and Zr_5Sn_4. The X-ray diffraction patterns confirmed the existence of a solid solution formed by silver atoms replacing tin atoms in the Zr_5Sn_4 compound. The results of EPMA and crystallographic data for some ternary Zr–Ag–Sn alloys, annealed at 770 K are presented in Fig. 1 and Table 2. Electron microprobe analysis of the sample $Zr_{45}Ag_{25}Sn_{30}$ (Fig. 1a) showed that the maximum solubility of Ag in Zr_5Sn_4 is ~11.5 at.% (Table 2), for this reason we can describe the final formula of the solid solution as $Zr_5Ag_xSn_{4-x}$, where x = 0.0-1.0. Fig. 1a shows the presence of large grains in different orientations of the Zr_5AgSn_3 phase, which is in equilibrium with silver. The compositions and cell parameters of the $Zr_5Ag_xSn_{4-x}$ solid solution are listed in Table 3.

The Zr_5AgSn_3 compound is also in equilibrium with other binary compounds in the ternary system (Fig. 2). The sample of composition $Zr_{20}Ag_{60}Sn_{20}$ (Fig. 1b) is located in a two-phase region and is in equilibrium with the Zr_5AgSn_3 and $Ag_{0.8}Sn_{0.2}$ phases. The sample with composition $Zr_{40}Ag_{40}Sn_{20}$ contains three phases (Fig. 1c): Zr_5AgSn_3, ZrAg and Ag (confirmed by analysis of the corresponding powder pattern). In the alloy $Zr_{20}Ag_{40}Sn_{40}$ the grains of Zr_5AgSn_3 are very small, and not visible (Fig. 1d), but we observed this phase in the X-ray diffraction pattern. Electron microprobe analysis of this sample indicated that, between the large grains of the main phase $Ag_{0.8}Sn_{0.2}$, small grains of the binary compound $ZrSn_2$ exist. In the sample $Zr_{70}Ag_8Sn_{22}$ the ternary phase Zr_5AgSn_3 is in equilibrium with Zr (Fig. 1e).

In the Zr–Ag–Sn ternary system silver dissolves up to ~10.5 at.% of tin and ~2 at.% of zirconium. At 770 K the Sn-rich part of the binary Ag–Sn system is in the liquid state, which continues in the ternary field up to ~8 at.% of Zr. Three phase equilibria, lattice

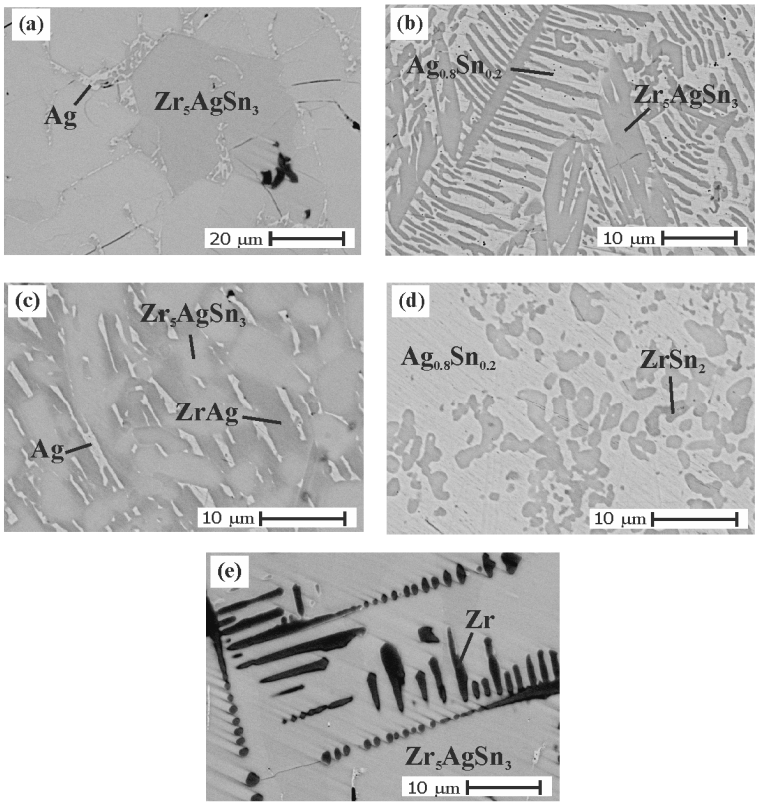

Fig. 1 Microstructures of alloys:
a) $Zr_{45}Ag_{25}Sn_{30}$ (white – Ag, gray – Zr_5AgSn_3);
b) $Zr_{20}Ag_{60}Sn_{20}$ (white – $Ag_{0.8}Sn_{0.2}$, gray – Zr_5AgSn_3),
c) $Zr_{40}Ag_{40}Sn_{20}$ (white – Ag, gray – ZrAg, gray light – Zr_5AgSn_3),
d) $Zr_{20}Ag_{40}Sn_{40}$ (white – $Ag_{0.8}Sn_{0.2}$, gray – $ZrSn_2$);
e) $Zr_{70}Ag_8Sn_{22}$ (gray – Zr_5AgSn_3, black – Zr).

Table 3 Composition and cell parameters for samples in the Zr_5Sn_4–Zr_5AgSn_3 region.

Composition	Lattice parameters, nm		V, nm^3
	a	*c*	
$Zr_{55.6}Sn_{44.4}$ (Zr_5Sn_4)	0.8456(4)	0.5784(5)	0.3582
$Zr_{55.6}Ag_{2.2}Sn_{42.2}$	0.8452(3)	0.5778(5)	0.3573
$Zr_{55.6}Ag_{4.4}Sn_{40.0}$	0.8450(2)	0.5777(5)	0.3572
$Zr_{55.6}Ag_{6.7}Sn_{37.7}$	0.8448(9)	0.5775(9)	0.3569
$Zr_{55.6}Ag_{8.9}Sn_{35.5}$	0.8446(2)	0.5770(3)	0.3565
$Zr_{55.6}Ag_{11.1}Sn_{33.3}$	0.8445(3)	0.5768(5)	0.3563
$Zr_{55.6}Ag_{13.3}Sn_{31.1}$	0.8445(2)	0.5767(4)	0.3562

parameters and phase compositions of the Zr–Ag–Sn system at 770 K are presented in Table 4 and Fig. 2.

3.2. Isothermal section of the Hf–Ag–Sn system

The phase equilibria of the Hf–Ag–Sn ternary system at 870 K were investigated based on X-ray diffraction and electron probe microanalysis of 35 binary and ternary alloys.

The phase diagrams of the binary systems Hf–Ag, Ag–Sn and Hf–Sn, which delimit the ternary Hf–Ag–Sn system, are reported in [14,17-18,20-27]. The presence of almost all of the binary compounds reported at 870 K in the Hf–Ag (Hf_2Ag, HfAg), Ag–Sn ($Ag_{0.8}Sn_{0.2}$) and Hf–Sn ($HfSn_2$, HfSn, Hf_5Sn_4, Hf_5Sn_3) systems, was confirmed. Crystal structure data of the unary and binary phases in the Hf–Ag, Ag–Sn and Hf–Sn systems at 870 K are given in Table 5.

The solubility of the third component in the binary compounds is less than 1-2 at.%. The X-ray diffraction patterns confirmed the existence of a solid solution formed by the substitution of silver for tin

Table 4 Three phase equilibria, lattice parameters and phase compositions of samples in the Zr–Ag–Sn system at 770 K.

Phase region	Phase	Structure type	Lattice parameters, nm			Composition, at.%		
			a	*b*	*c*	Zr	Ag	Sn
(Ag) +	(Ag)	Cu	0.4095(1)	–	–	–	89.5	10.5
Zr_5AgSn_3 +	Zr_5AgSn_3	Hf_5CuSn_3	0.8445(3)	–	0.5768(5)	55.6	11.1	33.3
$Ag_{0.8}Sn_{0.2}$	$Ag_{0.8}Sn_{0.2}$	Mg	0.2956(1)	–	0.4752(2)	–	87.7	12.3
$Ag_{0.8}Sn_{0.2}$ +	$Ag_{0.8}Sn_{0.2}$	Mg	0.2980(2)	–	0.4750(2)	–	77.8	22.2
Zr_5AgSn_3 +	Zr_5AgSn_3	Hf_5CuSn_3	0.8414(1)	–	0.5762(2)	55.6	11.1	33.3
$ZrSn_2$	$ZrSn_2$	$TiSi_2$	0.5612(1)	0.9543(1)	0.9881(1)	33.3	–	66.7
$Ag_{0.8}Sn_{0.2}$ +	$Ag_{0.8}Sn_{0.2}$	Mg	0.2983(2)	–	0.4750(2)	–	77.8	22.2
$ZrSn_2$ +	$ZrSn_2$	$TiSi_2$	0.5610(1)	0.9542(1)	0.9881(1)	33.3	–	66.7
L	L					~ 8	~ 10	~ 82
$ZrSn_2$ +	$ZrSn_2$	$TiSi_2$	0.5612(1)	0.9543(1)	0.9881(1)	33.3	–	66.7
Zr_5AgSn_3 +	Zr_5AgSn_3	Hf_5CuSn_3	0.8414(1)	–	0.5762(2)	55.6	11.1	33.3
Zr_5Sn_4	Zr_5Sn_4	Ti_5Ga_4	0.8456(4)	–	0.5784(5)	55.6	–	44.4
Zr_5Sn_3 +	Zr_5Sn_3	Mn_5Si_3	0.8431(3)	–	0.5723(4)	62.5	–	37.5
Zr_5AgSn_3 +	Zr_5AgSn_3	Hf_5CuSn_3	0.8414(1)	–	0.5762(2)	55.6	11.1	33.3
$Zr_{3.2}Sn_{0.8}$	$Zr_{3.2}Sn_{0.8}$	Cr_3Si	0.5622(3)	–	–	80.0	–	20.0
$Zr_{3.2}Sn_{0.8}$ +	$Zr_{3.2}Sn_{0.8}$	Cr_3Si	0.5622(3)	–	–	80.0	–	20.0
Zr_5AgSn_3 +	Zr_5AgSn_3	Hf_5CuSn_3	0.8414(1)	–	0.5762(2)	55.6	11.1	33.3
(Zr)	(Zr)	Mg	0.3218(1)	–	0.5161(3)	100	–	–
(Zr) +	(Zr)	Mg	0.3218(1)	–	0.5161(3)	100	–	–
Zr_5AgSn_3 +	Zr_5AgSn_3	Hf_5CuSn_3	0.8414(1)	–	0.5762(2)	55.6	11.1	33.3
Zr_2Ag	Zr_2Ag	Zr_2Cu	0.3246(2)	–	1.1923(4)	67.1	32.9	–
Zr_2Ag +	Zr_2Ag	Zr_2Cu	0.3246(2)	–	1.1923(4)	66.1	33.9	–
Zr_5AgSn_3 +	Zr_5AgSn_3	Hf_5CuSn_3	0.8414(1)	–	0.5762(2)	55.6	11.1	33.3
ZrAg	ZrAg	TiCu	0.3469(2)	–	0.6589(3)	51.7	48.3	–
ZrAg +	ZrAg	TiCu	0.3469(2)	–	0.6589(3)	48.1	51.9	–
Zr_5AgSn_3 +	Zr_5AgSn_3	Hf_5CuSn_3	0.8414(1)	–	0.5762(2)	55.6	11.1	33.3
(Ag)	(Ag)	Cu	0.4095(1)	–	–	1.4	96.8	1.8

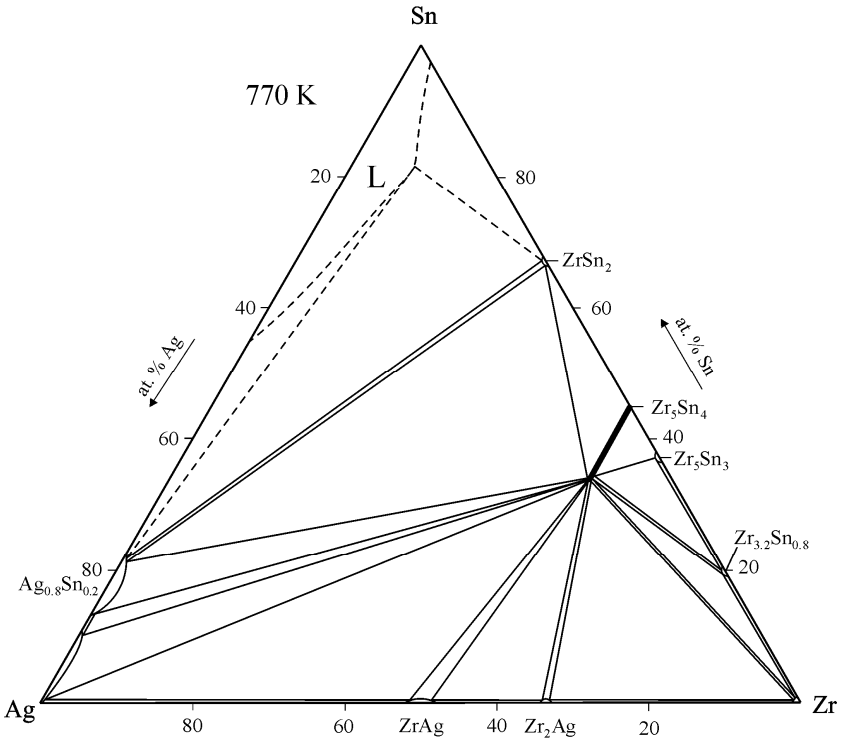

Fig. 2 Isothermal section of the Zr–Ag–Sn phase diagram at 770 K.

Table 5 Crystallographic characteristics of unary and binary phases in the Hf–Ag, Ag–Sn and Hf–Sn systems at 870 K.

Phase	Pearson symbol	Space group	Structure type	Lattice parameters, nm		Reference
				a	*c*	
(Hf)	*hP*2	*P*6$_3$/*mmc*	Mg	0.3194	0.5052	[23]
				0.3181(3)	0.5060(6)	this work
Hf_2Ag	*tI*6	*I*4/*mmm*	Zr_2Cu	0.319	1.183	[24]
				0.3195(4)	1.1828(5)	this work
HfAg	*tP*4	*P*4/*nmm*	TiCu	0.342	0.657	[24]
				0.3427(3)	0.6362(4)	this work
(Ag)	*cF*4	*Fm*-3*m*	Cu	0.4080	–	[17]
$Ag_{1-x}Sn_x$ (x = 0.0-0.1)	*cF*4	*Fm*-3*m*	Cu	0.4065(3)-0.4095(4)	–	this work
$Ag_{0.8}Sn_{0.2}$ (12.3-20.0 at.% Sn)	*hP*2	*P*6$_3$/*mmc*	Mg	0.29658	0.47824	[17]
				0.2959(1)-0.2979(2)	0.4751(2)-0.4750(2)	this work
(Sn)	*tI*4	*I*4$_1$/*amd*	Sn	0.58300	0.31802	[18]
				0.5814(2)	0.3173(1)	this work
$HfSn_2$	*hP*9	*P*6$_2$22	$CrSi_2$	0.547	0.760	[25]
				0.5466(6)	0.7581(7)	this work
HfSn	*cP*8	*P*2$_1$3	FeSi	0.5594	–	[26]
				0.5593(5)	0.7589(7)	this work
Hf_5Sn_4	*hP*18	*P*6$_3$/*mcm*	Ti_5Ga_4	0.8695	0.5875	[20]
				0.8334(5)	0.5694(6)	this work
Hf_5Sn_3	*hP*16	*P*6$_3$/*mcm*	Mn_5Si_3	0.8376	0.5737	[27]
				0.8321(3)	0.5675(4)	this work

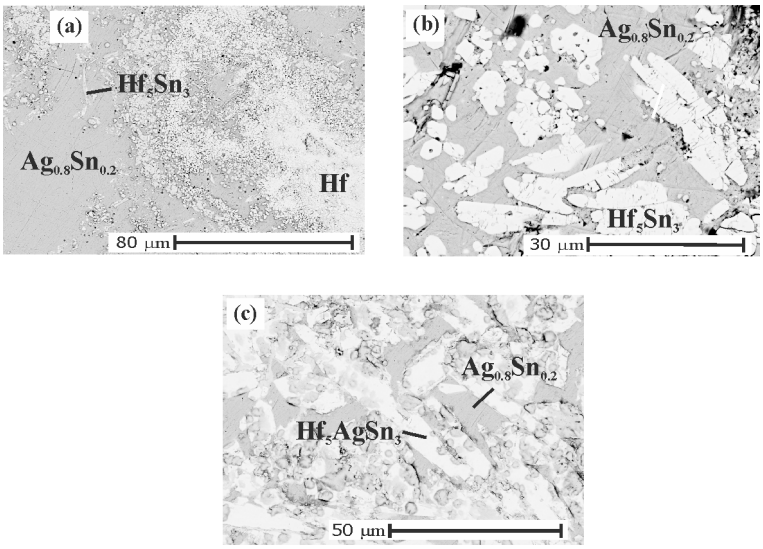

Fig. 3 Microstructures of alloys:
a) $Hf_{20}Ag_{60}Sn_{20}$ (white – Hf, gray light – Hf_5AgSn_3, gray – $Ag_{0.8}Sn_{0.2}$);
b) $Hf_{30}Ag_{45}Sn_{25}$ (gray – $Ag_{0.8}Sn_{0.2}$, white – Hf_5Sn_3);
c) HfAgSn (gray – $Ag_{0.8}Sn_{0.2}$, white – Hf_5AgSn_3).

atoms in the Hf_5Sn_4 compound. The compositions and cell parameters for the solid solution $Hf_5Ag_xSn_{4-x}$ (x = 0.0-1.0) samples are listed in Table 6. Reduction of the volume and cell parameters is observed with increasing silver content in the alloys. The mechanism of replacement of Sn by Ag atoms appears to be similar to that described for the $Zr_5Ag_xSn_{4-x}$ (x = 0.0-1.0) solid solution. The ternary alloys with composition close to the $Hf_5Ag_xSn_{4-x}$ (x = 0.0-1.0) solid solution are air-sensitive.

The results of EPMA and crystallographic data for some Hf–Ag–Sn alloys, annealed at 870 K are presented in Table 7 and Fig. 3. Three phase equilibria, lattice parameters and the isothermal section of the Hf–Ag–Sn system at 870 K are presented in Table 8 and Fig. 4, respectively.

Table 6 Composition and cell parameters for samples in the Hf_5Sn_3–Hf_5AgSn_3–Hf_5Sn_4 region.

Composition	Lattice parameters, nm		V, nm^3
	a	*c*	
$Hf_{62.5}Sn_{37.5}$ (Hf_5Sn_3)	0.8321(3)	0.5675(4)	0.3403
$Hf_{55.6}Sn_{44.4}$ (Hf_5Sn_4)	0.8334(5)	0.5694(6)	0.3425
$Hf_{62.0}Ag_{3.3}Sn_{34.7}$	0.8302(3)	0.5673(3)	0.3386
$Hf_{55.0}Ag_{3.3}Sn_{41.7}$	0.8305(2)	0.5680(3)	0.3393
$Hf_{59.5}Ag_{6.7}Sn_{33.8}$	0.8295(5)	0.5665(5)	0.3376
$Hf_{55.0}Ag_{6.7}Sn_{38.3}$	0.8294(4)	0.5665(6)	0.3375
$Hf_{55.6}Ag_{11.1}Sn_{33.3}$	0.8281(7)	0.5655(8)	0.3358

Table 7 EPMA and crystallographic data for selected Hf–Ag–Sn alloys annealed at 870 K.

Nominal composition	Phase	Structure type	Lattice parameters, nm			EPMA, at.%		
			a	*b*	*c*	Hf	Ag	Sn
$Hf_{24}Ag_{70}Sn_6$	HfAg	TiCu	0.3432(7)	–	0.6337(8)			
	(Ag)	Cu	0.4057(8)	–	–			
$Hf_{70}Ag_{25}Sn_5$	Hf	Mg	0.3181(3)	–	0.5060(6)			
	$Ag_{0.8}Sn_{0.2}$	Mg						
	Hf_2Ag	Zr_2Cu	0.3195(4)	–	1.1828(5)			
$Hf_{20}Ag_{60}Sn_{20}$ (a)	Hf_5Sn_3	Mg_5Si_3	0.8324(3)	–	0.5691(4)			
	$Ag_{0.8}Sn_{0.2}$	Mg	0.2976(5)	–	0.4760(7)	–	79.90	20.10
	Hf	Mg	0.3189(3)	–	0.5055(5)	93.02	–	6.98
$Hf_{30}Ag_{45}Sn_{25}$ (b)	Hf_5Sn_3	Mg_5Si_3	0.8325(5)	–	0.5693(5)	62.35	0.12	37.53
	$Ag_{0.8}Sn_{0.2}$	Mg	0.2975(4)	–	0.4760(5)	0.31	82.08	17.61
$Hf_{50}Ag_{18}Sn_{32}$	Hf_5AgSn_3	Hf_5CuSn_3	0.8280(6)	–	0.5656(5)			
	Hf_5Sn_3	Mg_5Si_3	0.8320(3)	–	0.5673(4)			
	$Ag_{0.8}Sn_{0.2}$	Mg	0.2953(2)	–	0.4788(3)			
$Hf_{33.3}Ag_{33.3}Sn_{33.3}$ (c)	$Hf_5Ag_xSn_3$	Hf_5CuSn_3	0.8299(2)	–	0.5672(3)	55.09	4.51	40.40
	$Ag_{0.8}Sn_{0.2}$	Mg	0.2990(4)	–	0.4787(6)	–	79.70	20.30
$Hf_{30}Ag_{30}Sn_{40}$	$Hf_5Ag_xSn_3$	Hf_5CuSn_3	0.8304(3)	–	0.5676(3)			
	$Ag_{0.8}Sn_{0.2}$	Mg	0.2971(1)	–	0.4791(3)			
	$HfSn_2$	$CrSi_2$	0.5470(3)	–	0.7594(7)			

* a, b, c correspond to samples in Fig. 3.

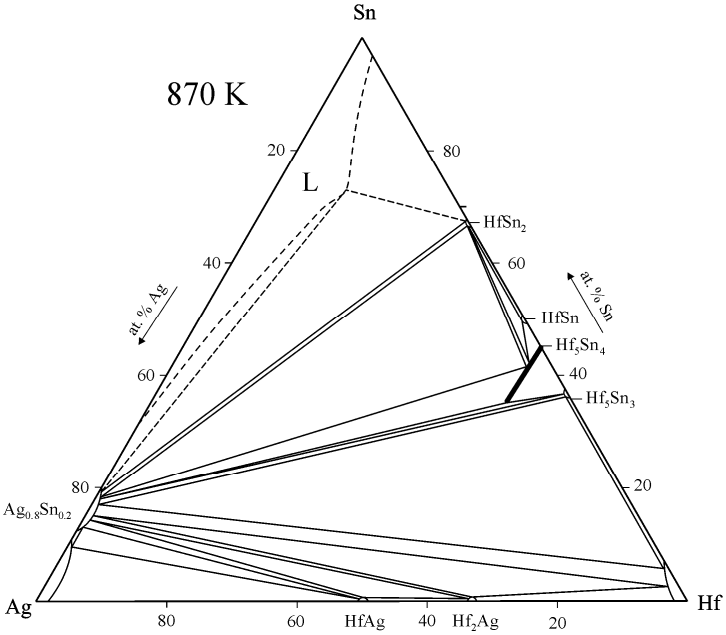

Fig. 4 Isothermal section of the phase diagram of the Hf–Ag–Sn system at 870 K.

Table 8 Three phase equilibria, lattice parameters and phase composition of samples in the Hf–Ag–Sn system at 870 K.

Phase region	Phase	Structure type	Lattice parameters, nm			Composition		
			a	*b*	*c*	Hf	Ag	Sn
(Ag) +	(Ag)	Cu	0.4065(3)	–	–	–	89.2	10.8
HfAg+	HfAg	TiCu	0.3427(3)	–	0.6362(4)	50.0	50.0	–
$Ag_{0.8}Sn_{0.2}$	$Ag_{0.8}Sn_{0.2}$	Mg	0.2959(1)	–	0.4751(2)	–	87.5	12.5
HfAg +	HfAg	TiCu	0.3427(3)	–	0.6362(4)	50.0	50.0	–
$Ag_{0.8}Sn_{0.2}$ +	$Ag_{0.8}Sn_{0.2}$	Mg	0.2963(1)	–	0.4752(2)	–	86.0	14.0
Hf_2Ag	Hf_2Ag	Zr_2Cu	0.3195(4)	–	1.1828(5)	66.7	33.3	–
Hf_2Ag +	Hf_2Ag	Zr_2Cu	0.3195(4)	–	1.1828(5)	66.7	33.3	–
$Ag_{0.8}Sn_{0.2}$ +	$Ag_{0.8}Sn_{0.2}$	Mg	0.2963(1)	–	0.4752(2)	–	86.0	14.0
Hf	(Hf)	Mg	0.3189(3)	–	0.5055(5)	95.8	1.9	2.3
Hf +	(Hf)	Mg	0.3189(3)	–	0.5055(5)	93.6	0.6	5.8
$Ag_{0.8}Sn_{0.2}$ +	$Ag_{0.8}Sn_{0.2}$	Mg	0.2969(3)	–	0.4750(5)	0.8	83.1	16.1
Hf_5Sn_3	Hf_5Sn_3	Mn_5Si_3	0.8321(3)	–	0.5675(4)	62.5	–	37.5
Hf_5Sn_3 +	Hf_5Sn_3	Mn_5Si_3	0.8321(3)	–	0.5675(4)	62.5	–	37.5
$Ag_{0.8}Sn_{0.2}$ +	$Ag_{0.8}Sn_{0.2}$	Mg	0.2969(3)	–	0.4750(5)	0.8	83.1	16.1
Hf_5AgSn_3	Hf_5AgSn_3	Hf_5CuSn_3	0.8281(7)	–	0.5655(8)	55.6	11.1	33.3
Hf_5AgSn_3+	Hf_5AgSn_3	Hf_5CuSn_3	0.8281(7)	–	0.5655(8)	55.6	11.1	33.3
$Ag_{0.8}Sn_{0.2}$ +	$Ag_{0.8}Sn_{0.2}$	Mg	0.2969(3)	–	0.4750(5)	0.8	83.1	16.1
$HfSn_2$	$HfSn_2$	$CrSi_2$	0.5466(6)	–	0.7581(7)	33.3	–	66.7
$Ag_{0.8}Sn_{0.2}$ +	$Ag_{0.8}Sn_{0.2}$	Mg	0.2979(2)	–	0.4750(2)	–	79.9	20.1
L +	L					~ 11	~ 16	~ 73
$HfSn_2$	$HfSn_2$	$CrSi_2$	0.5466(6)	–	0.7581(7)	33.3	–	66.7
$HfSn_2$ +	$HfSn_2$	$CrSi_2$	0.5466(6)	–	0.7581(7)	33.3	–	66.7
Hf_5AgSn_3 +	Hf_5AgSn_3	Hf_5CuSn_3	0.8281(7)	–	0.5655(8)	55.6	11.1	33.3
HfSn	HfSn	FeSi	0.5593(5)	–	0.7589(7)	50.0	–	50.0
HfSn +	HfSn	FeSi	0.5593(5)	–	0.7589(7)	50.0	–	50.0
Hf_5AgSn_3 +	Hf_5AgSn_3	Hf_5CuSn_3	0.8281(7)	–	0.5655(8)	55.6	11.1	33.3
Hf_5Sn_4	Hf_5Sn_4	Ti_5Ga_4	0.8334(5)	–	0.5694(6)	55.6	–	44.4
Hf_5Sn_4 +	Hf_5Sn_4	Ti_5Ga_4	0.8334(5)	–	0.5694(6)	55.6	–	44.4
Hf_5AgSn_3 +	Hf_5AgSn_3	Hf_5CuSn_3	0.8281(7)	–	0.5655(8)	55.6	11.1	33.3
Hf_5Sn_3	Hf_5Sn_3	Mn_5Si_3	0.8321(3)	–	0.5675(4)	62.5	–	37.5

4. Conclusions

The isothermal sections of the Zr–Ag–Sn and Hf–Ag–Sn ternary systems were constructed at 770 K and 870 K, respectively. No ternary compounds form at the investigated temperatures of annealing. The homogeneity regions and cell parameters of the solid solutions $Zr_5Ag_xSn_{4-x}$ and $Hf_5Ag_xSn_{4-x}$ (x = 0.0-1.0) were determined using EMPA and X-ray powder diffraction.

References

[1] Y.V. Stadnyk, L.P. Romaka, V.K. Pecharsky, R.V. Skolozdra, *Neorg. Mater.* 31 (1995) 1422-1425.

[2] L. Romaka, Yu.V. Stadnyk, O.I. Bodak, *J. Alloys Compd*. 317-318 (2001) 347-349.

[3] Yu.V. Stadnyk, R.V. Skolozdra, *Metally* (1) (1994) 164-167.

[4] Yu.V. Stadnyk, L.P. Romaka, *J. Alloys Compd.* 316 (2001) 169-171.

[5] L.P. Romaka, N.O. Koblyuk, Yu.V. Stadnyk, D.P. Frankevych, R.V. Skolozdra, *Pol. J. Chem.* 72(7) (1998) 1154-1159.

[6] N. Koblyuk, L. Romaka, Yu. Stadnyk, P. Starodub, *Coll. Abstr. 10th Conf. "Lviv Chemical Readings"*, 2005, H27.

[7] G.A. Melnyk, D. Fruchart, L.P. Romaka, Yu.V. Stadnyk, R.V. Skolozdra, J. Tobola, *J. Alloys Compd.* 267 (1998) L1-L3.

[8] V.A. Romaka, V.V. Romaka, Yu.V. Stadnyk, *Intermetallic Semiconductors: Properties and Applications*, Lviv, Lviv Polytechnic Publishing House, 2010, 508 p.

[9] V.A. Romaka, Yu.V. Stadnyk, V.V. Romaka, D. Fruchart, V.F. Chekurin, A.M. Horyn, *Semicond.* 41(9) (2007) 1041-1047.

[10] Y.-L. Kim, S.-J. Lee, H.-K. Baik, S.-M. Lee, *J. Power Sources* 119-121 (2003) 106-109.

[11] L.G. Akselrud, Yu.N. Grun, P.Yu. Zavalii, V.K. Pecharsky, V.S. Fundamensky, *Coll. Abstr. 12 Eur. Crystallogr. Meeting*, Moscow, 1989, Vol. 3, 155 p.
[12] W. Kraus, G. Nolze, *PowderCell for Windows* (version 2.4), Federal Institute for Materials Research and Testing, Berlin, 2000.
[13] J. Rodriguez-Carvajal, *FULLPROF: A Program for Rietveld Refinement and Pattern Matching Analysis*, version 3.5d, Laboratoire Léon Brillouin (CEA–CNRS), Saclay, France, 1998.
[14] N. Karlsson, *Acta Chem. Scand.* 6 (1952) 1424-1430.
[15] A. Raman, K. Schubert, *Z. Metallkd.* 55 (1964) 798-804.
[16] Z. Kanghou, Z. Huaiyhi, Z. Yuehua, *J. Less-Common Met.* 138 (1988) 173-177.
[17] H.W. King, T.B. Massalski, *Philos. Mag.* 6 (1961) 669-682.
[18] T.B. Massalski (Ed.), *Binary Alloy Phase Diagrams*, ASM International, Materials Park, Ohio, 1990.
[19] U-K. Young, J.D. Corbett, *Chem. Mater.* 2 (1990) 27-33.
[20] W. Rieger, H. Nowotny, F. Benesovsky, *Monatsh. Chem.* 96 (1965) 232-241.
[21] W. Rieger, H. Novotny, F. Benesovsky, *Monatsh. Chem.* 96 (1965) 98.
[22] M. Pötzschke, K. Schubert, *Z. Metallkd.* 53 (1962) 474-488.
[23] E. Rudy, F. Benesovsky, *Monatsh. Chem.* 92 (1961) 415-441.
[24] A. Raman, K. Schubert, *Z. Metallkd.* 55 (1964) 798-804.
[25] K. Schubert, H.G. Meissner, M. Pötzschke, W. Rossteutscher, E. Stolz, *Naturwissenschaften* 49 (1962) 57.
[26] O. Schob, E. Parthé, *Acta Crystallogr.* 17 (1964) 452-453.
[27] H. Boller, H. Nowotny, A. Wittmann, *Monatsh. Chem.* 91 (1960) 1174-1184.